Supporting Information for "A stochastic view of the 2020 Elazığ M_w6.8 earthquake"

Théa Ragon[1], Mark Simons[1], Quentin Bletery[2], Olivier Cavalié[2], Eric Fielding[3]

[1]Seismological Laboratory, California Institute of Technology, Pasadena, CA, USA.

[2]Université Côte dAzur, IRD, CNRS, Observatoire de la Côte dAzur, Géoazur, France.

[3]Jet Propulsion Laboratory, California Institute of Technology, Pasadena, CA, USA.

Contents of this file

1. Tables S1 to S2
2. Figures S1 to S12

0094-8276/20/$5.00

Width (km)	ρ **(mg/m^3)**	**Vp (km/s)**	**Vs (km/s)**	μ **(GPa)**	Std in μ
3.0	2.20	3.5	2.33	11.9	6
2.0	2.20	5.0	3.33	24.4	5
4.0	2.65	6.0	4.00	42.4	3.5
26.0	2.85	6.5	4.33	53.4	3
0.0	5.85	7.8	5.20	77.4	3

Table S1. Assumed elastic structure and assumed uncertainties (std = standard deviation). Poisson's ratio is assumed constant for each layer.

Satellite	**Orbital direction**	**Track**	**Interferogram pair**
ALOS 2	ascending	A182	2020/01/03 - 2020/01/31
ALOS 2	descending	D077	2019/03/03 - 2020/03/01
Sentinel 1A	ascending	TA116	2020/01/21 - 2020/01/27
Sentinel 1A	descending	TD123	2020/01/22 - 2020/01/28

Table S2. Interferometric pairs used for the study of the Elazig earthquake.

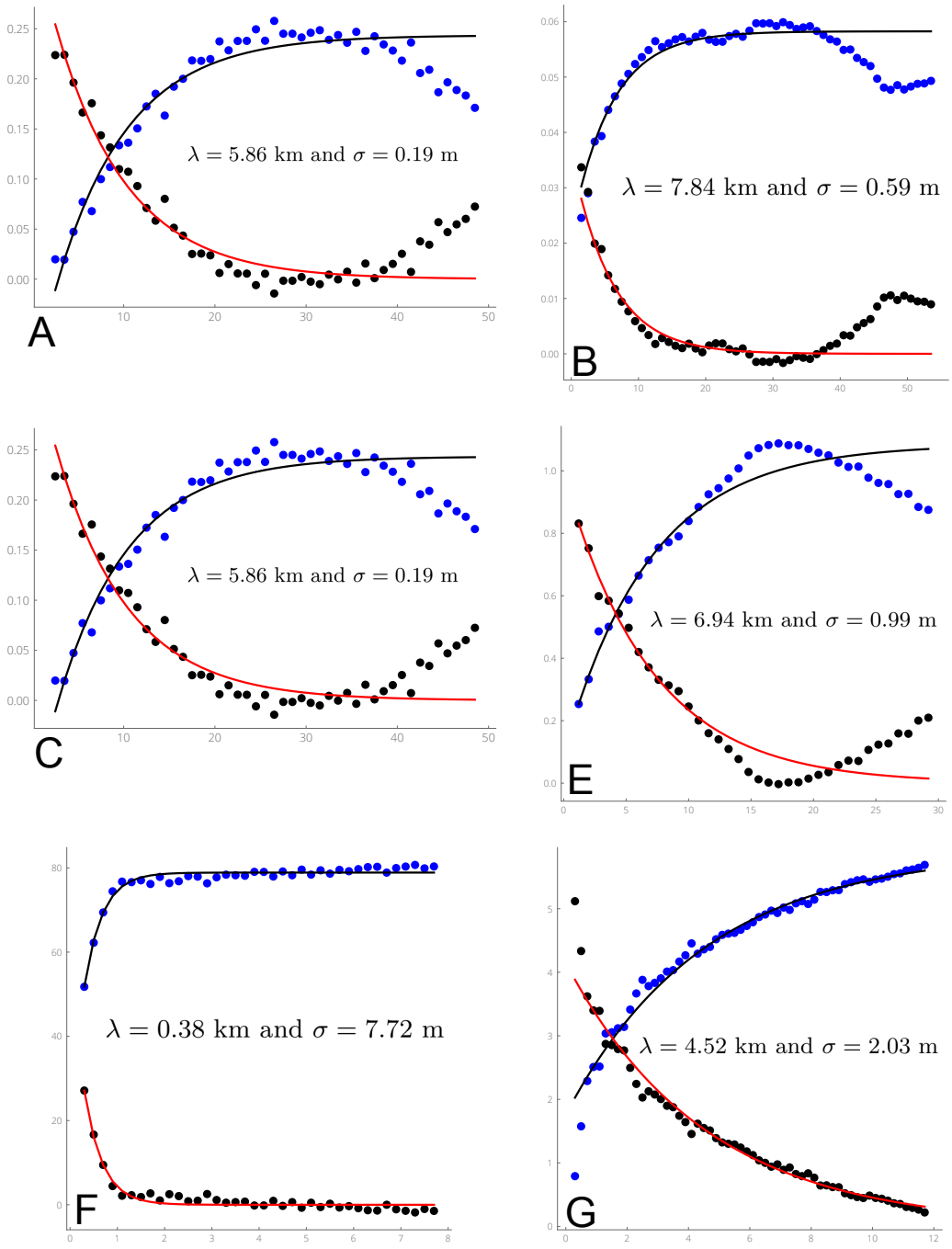

Figure S1. Empirical covariance functions (cm^2) in fonction of the distance between data points (km) for the pairs used in the study of the Elazig earthquake. A) Sentinel 1 Ascending. B) Sentinel 1 Descending. C) ALOS2 ascending. D) ALOS2 descending. E) ALOS2 descending pixel-offset. F) ALOS2 ascending pixel-offset. Radially symmetric empirical covariance functions (black points) and associated best fit exponential functions (red curve), as well as semivariograsm (black curve) are shown. For each interferogram, we compute the empirical covariance as a function of the inter-pixel distance and then fit an exponential function (Jolivet et al. 2012) such that σ and λ characterize $C(i,j) = \sigma^2 e^{-\frac{||i,j||^2}{\lambda}}$.

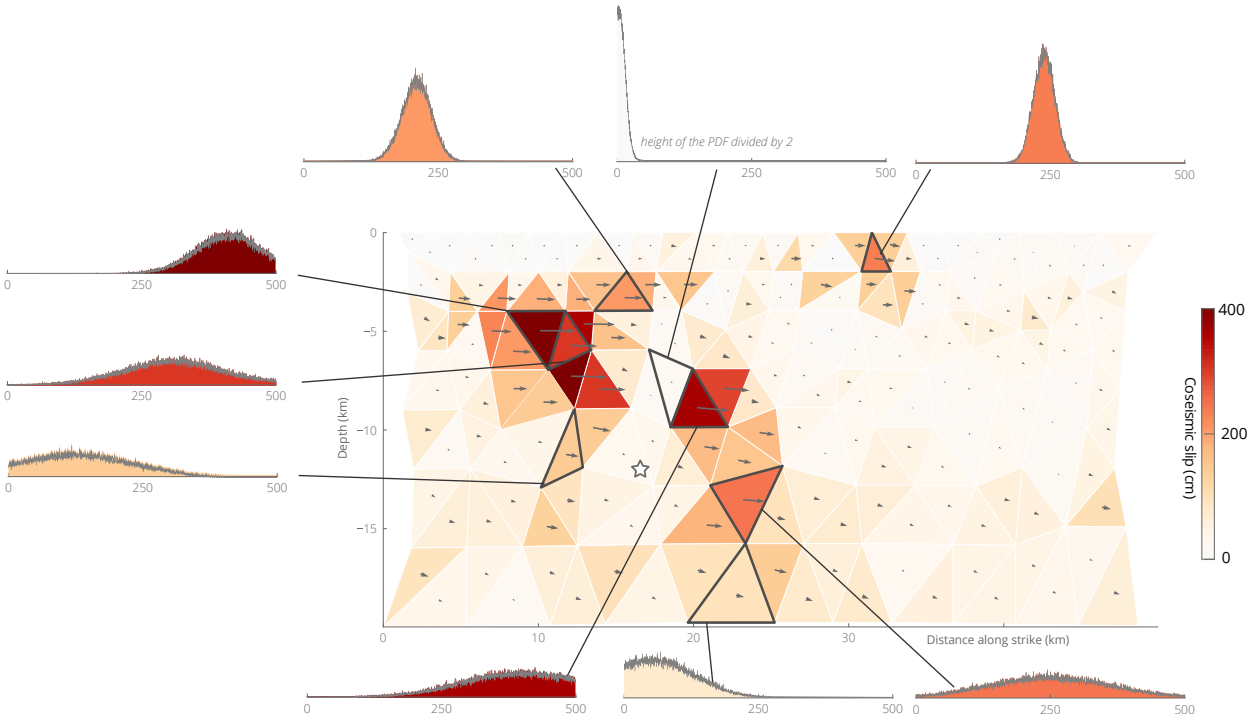

Figure S2. Posterior marginal probability density functions for selected strike-slip parameters of our preferred slip model.

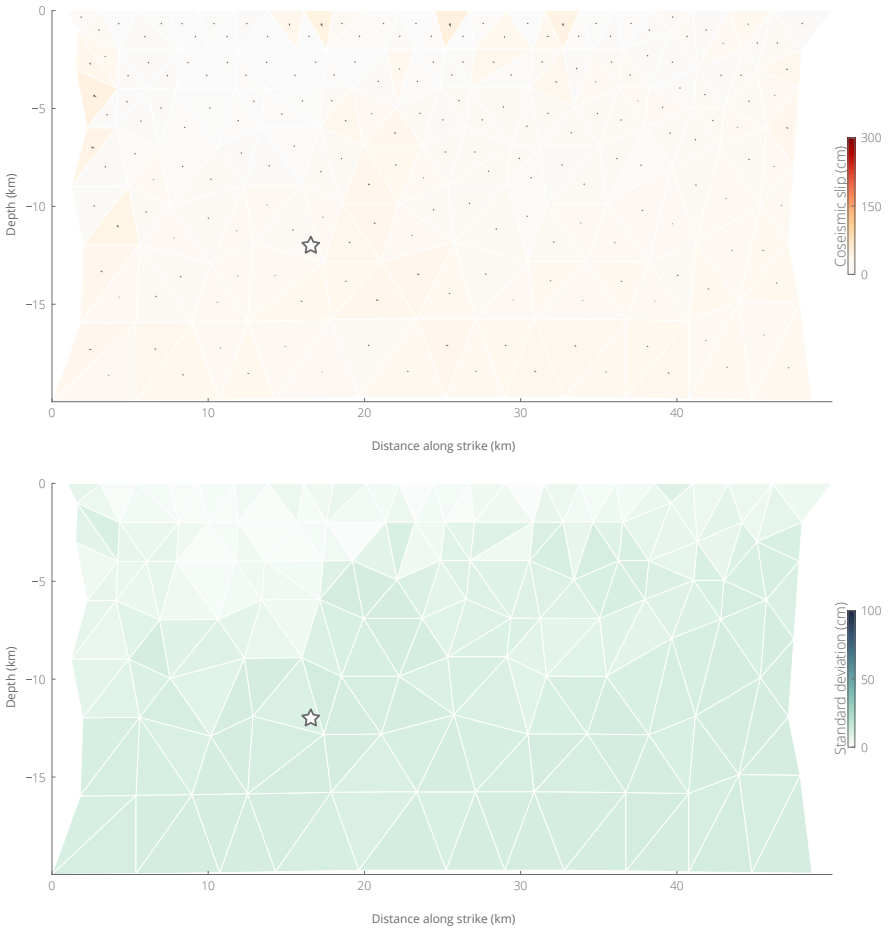

Figure S3. Inferred dip-slip amplitude (top) and associated standard deviation (bottom) for our preferred slip model.

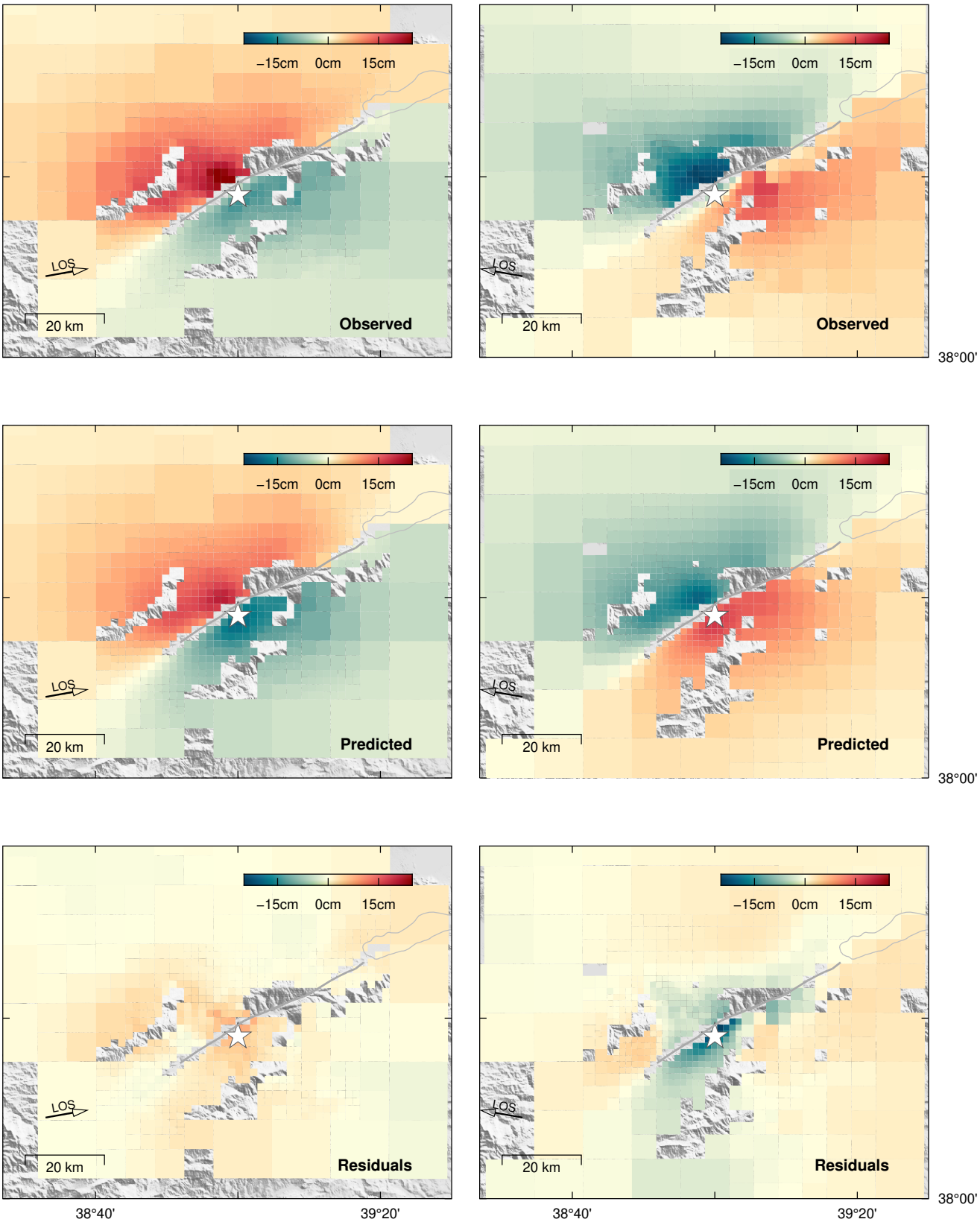

Figure S4. Observed and predicted surface displacement in the LOS direction for the Sentinel-1 ascending (left) and descending (right) interferograms. Predictions are inferred from the average model. The assumed fault trace is shown with a dark gray line.

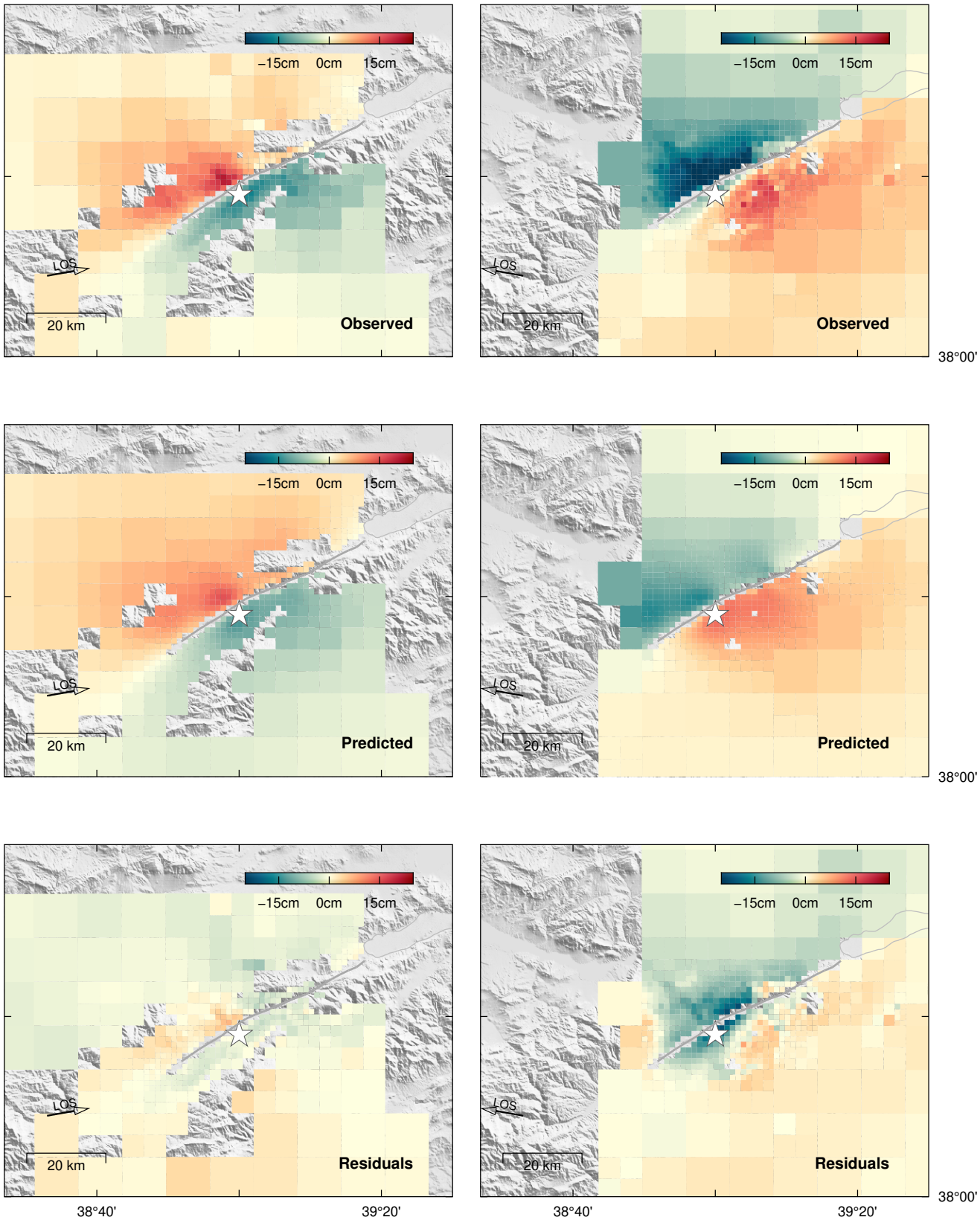

Figure S5. Observed and predicted surface displacement in the LOS direction for the ALOS 2 ascending (left) and descending (right) interferograms. Predictions are inferred from the average model. The assumed fault trace is shown with a dark gray line.

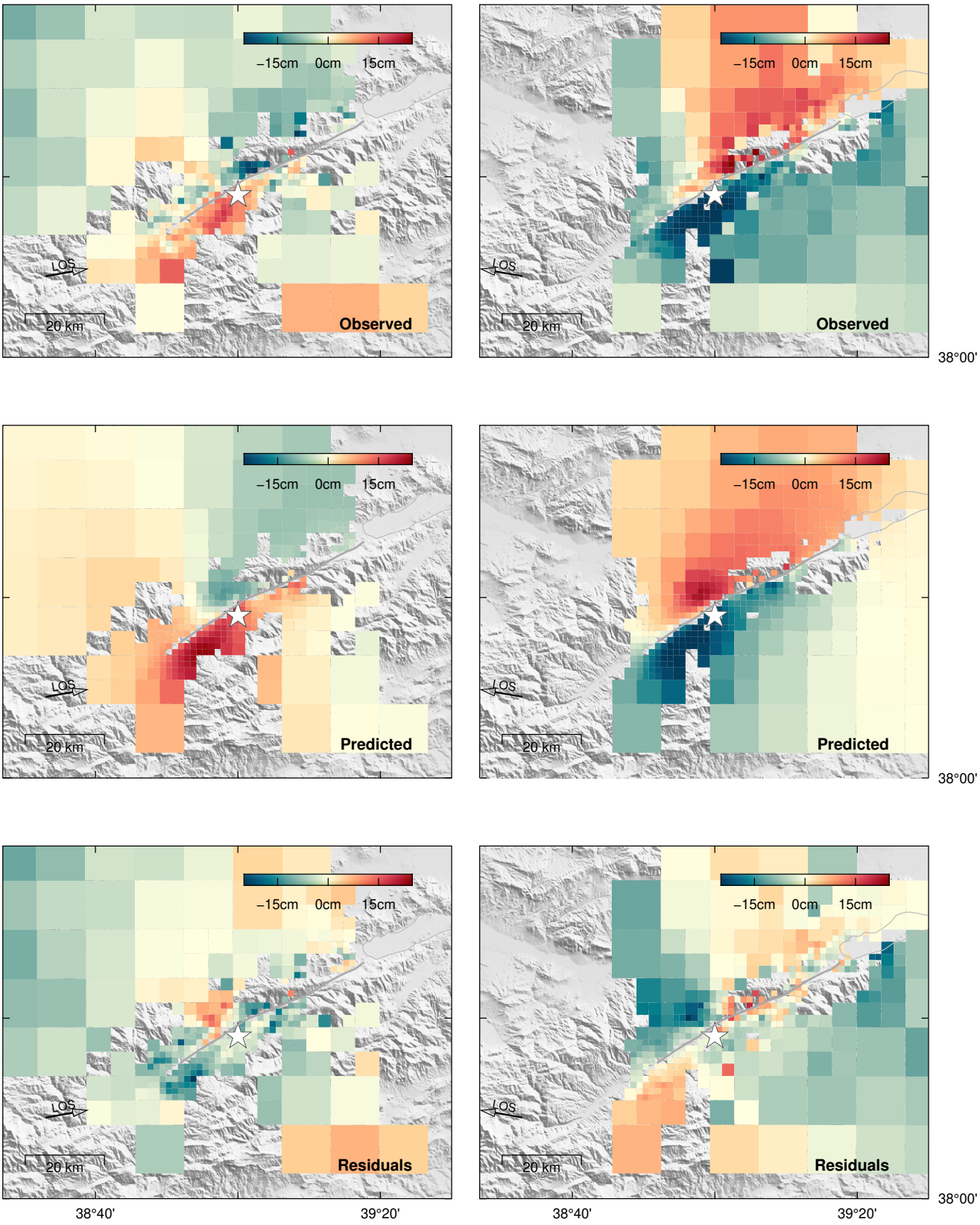

Figure S6. Observed and predicted pixel-offset surface displacement in the satellite azimuth direction for ALOS2 ascending (left) and descending (right) pairs. Predictions are inferred from the average model. The assumed fault trace is shown with a dark gray line.

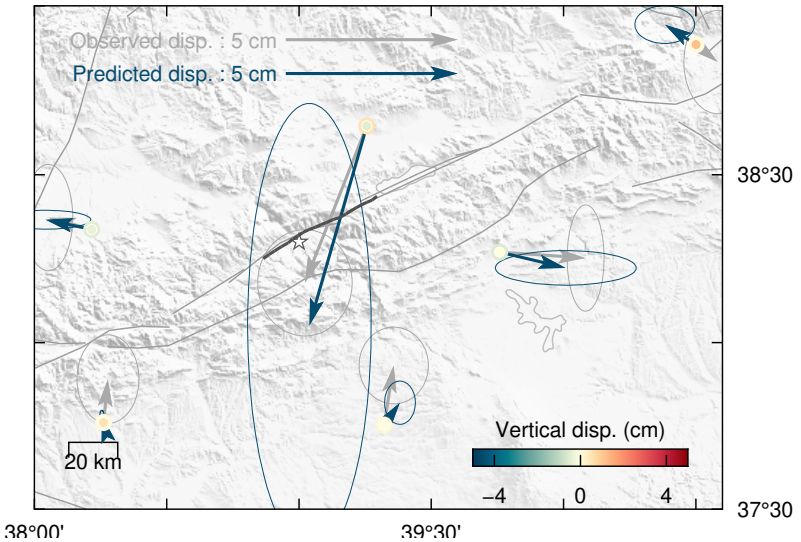

Figure S7. Observed and predicted surface displacement at the GNSS locations. Observed horizontal surface displacements are shown in gray with 90% confidence ellipses and vertical displacements as the inner amplitudes. Predicted horizontal displacements are shown in blue with 90% confidence ellipses and vertical displacements are the outer amplitudes. The assumed fault trace is shown with a dark gray line and the epicenter is the white star.

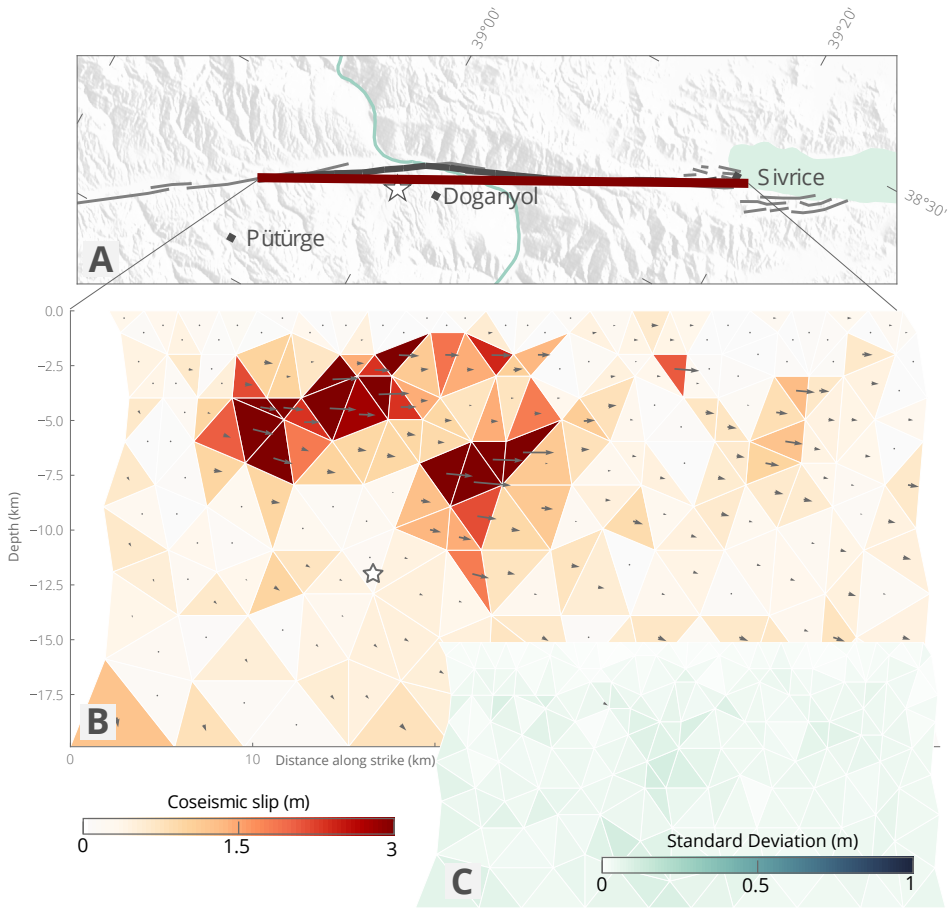

Figure S8. Inferred slip model and associated posterior uncertainty for the Elazığ earthquake, assuming a planar and vertical fault and no epistemic uncertainties. (a) Map view of the fault trace and local setting, the epicenter is the white star. (b) Depth view of the inferred total slip amplitudes and directions. (c) Standard deviation of the inferred strike-slip parameters.

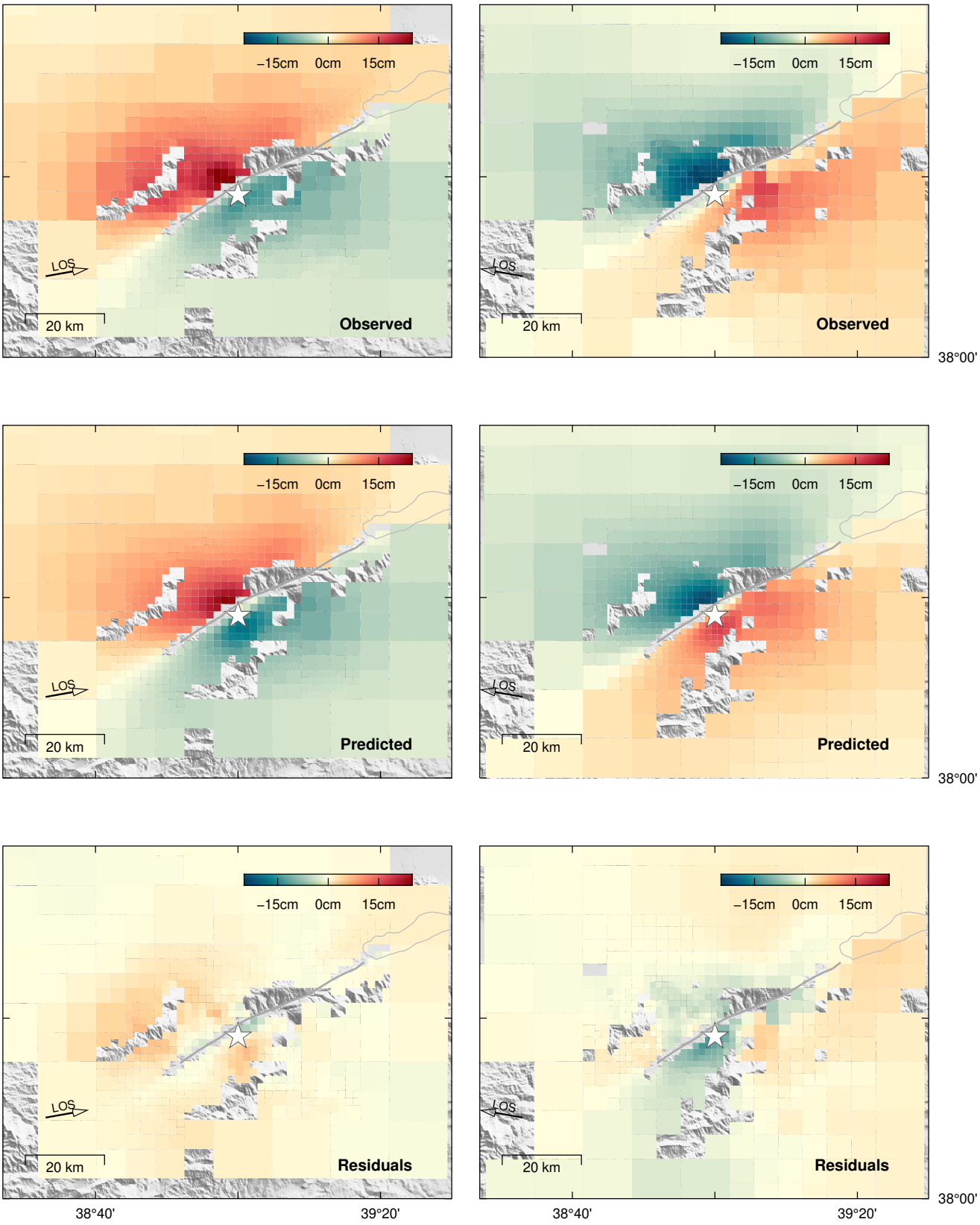

Figure S9. Observed and predicted surface displacement in the LOS direction for the Sentinel-1 ascending (left) and descending (right) interferograms. Predictions are inferred from the average model. The assumed fault trace is shown with a dark gray line.

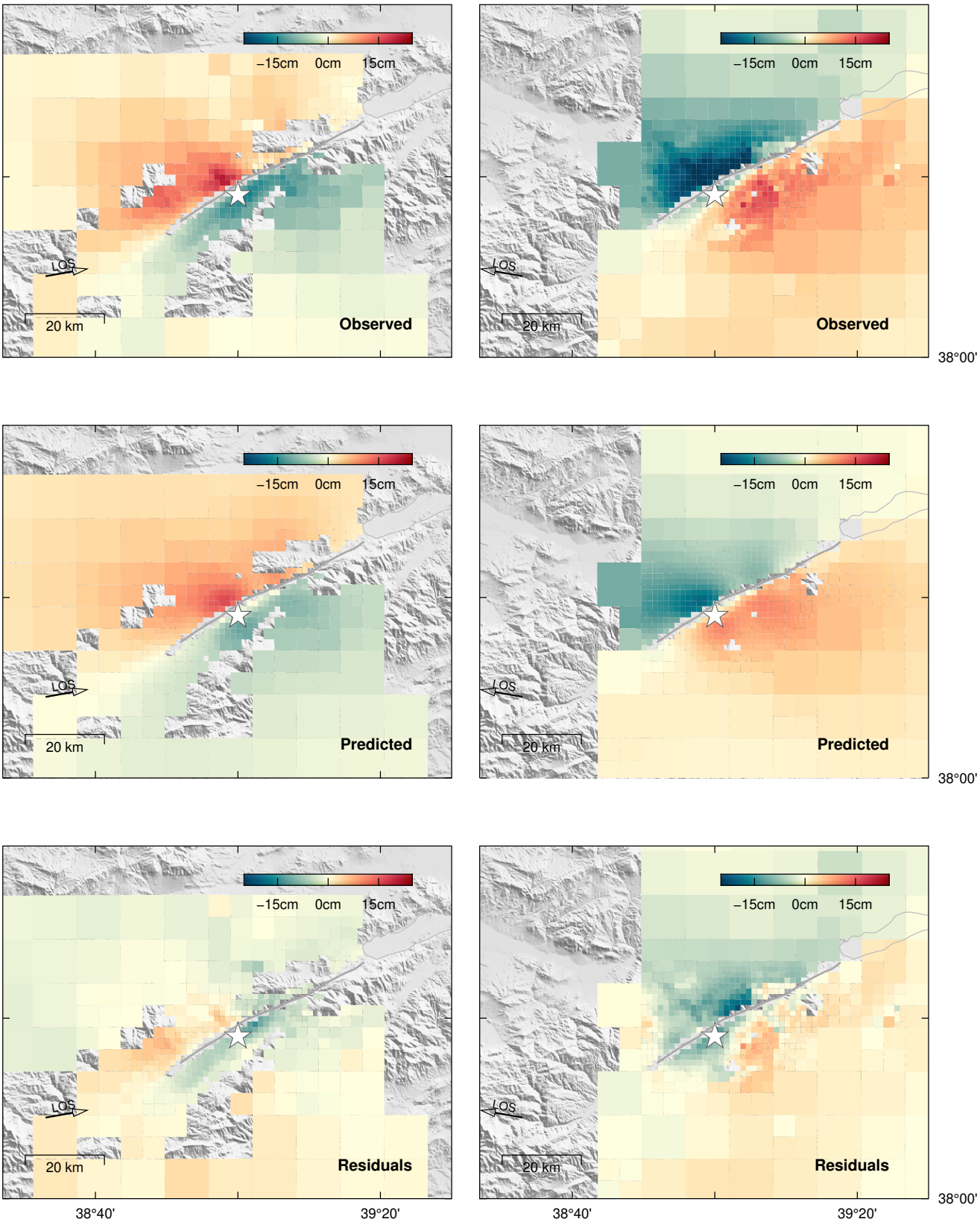

Figure S10. Observed and predicted surface displacement in the LOS direction for the ALOS 2 ascending (left) and descending (right) interferograms. Predictions are inferred from the average model. The assumed fault trace is shown with a dark gray line.

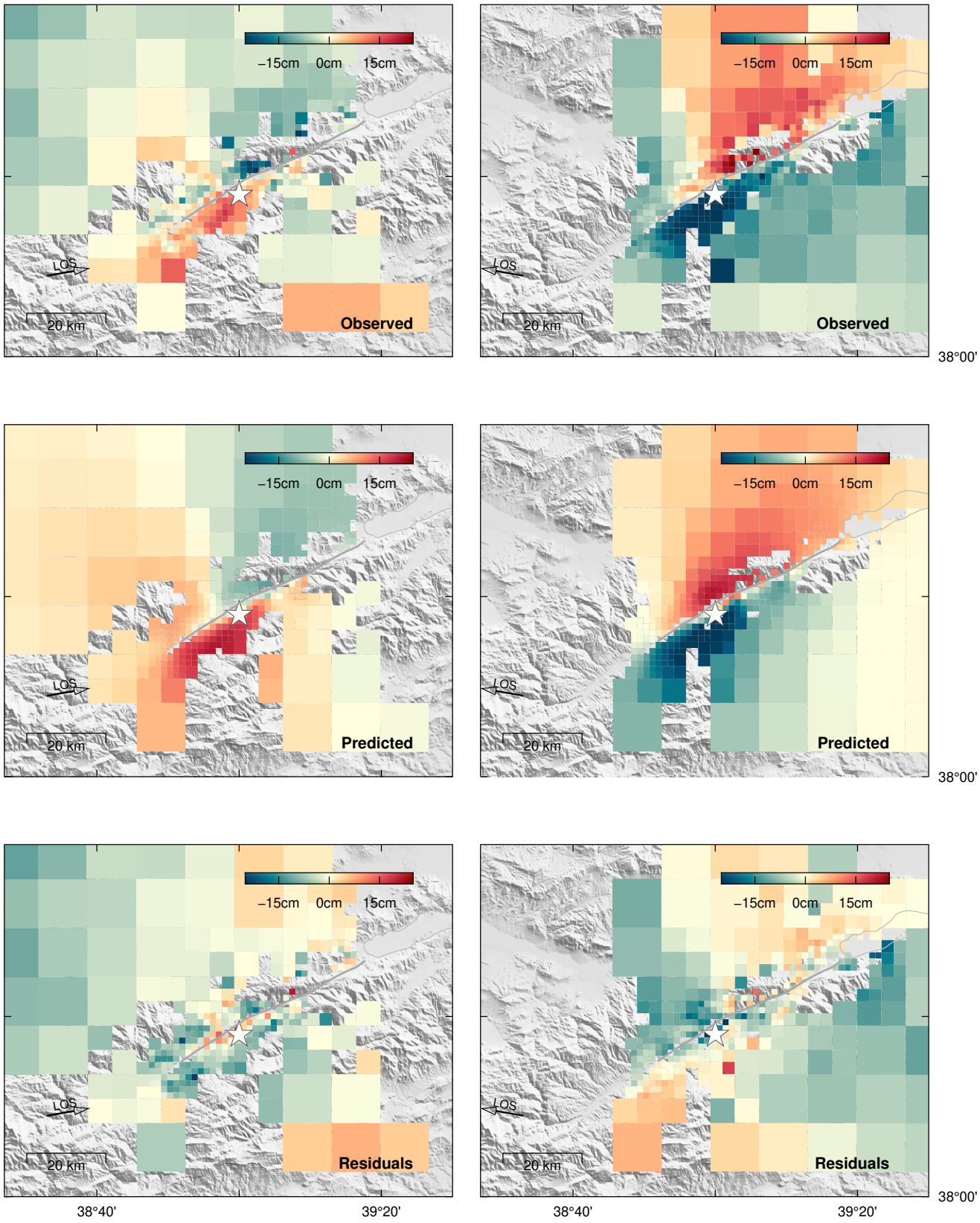

Figure S11. Observed and predicted pixel-offset surface displacement in the satellite azimuth direction for ALOS2 ascending (left) and descending (right) pairs. Predictions are inferred from the average model. The assumed fault trace is shown with a dark gray line.

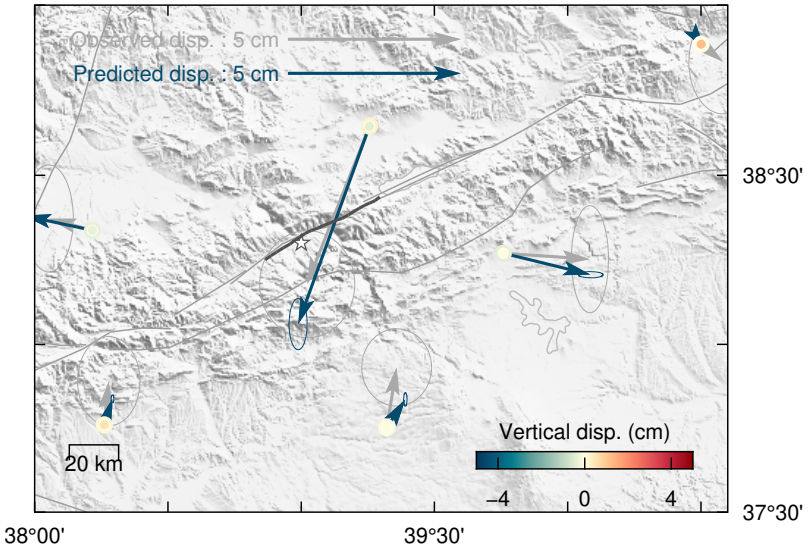

Figure S12. Observed and predicted surface displacement, assuming a planar fault, at the GNSS locations. Observed horizontal surface displacements are shown in gray with 90% confidence ellipses and vertical displacements as the inner amplitudes. Predicted horizontal displacements are shown in blue with 90% confidence ellipses and vertical displacements are the outer amplitudes. The assumed fault trace is shown with a dark gray line and the epicenter is the white star.